Sorting nexin 27 rescues neuroligin 2 from lysosomal degradation to control inhibitory synapse number

Caroline S. Binda, Yasuko Nakamura, Jeremy M. Henley and Kevin A. Wilkinson*

School of Biochemistry, Centre for Synaptic Plasticity, Biomedical Sciences Building, University of Bristol, Bristol, BS8 1TD, UK

*Corresponding author: Kevin.Wilkinson@bristol.ac.uk

Running title: SNX27 controls neuroligin 2 trafficking

Character count: 52,755

Abstract

Retromer is an evolutionarily conserved endosomal trafficking complex that mediates the retrieval of cargo proteins from a degradative pathway for sorting back to the cell surface. To promote cargo recycling, the core retromer trimer of VPS26, VPS29 and VPS35 recognises cargo either directly, or through an adaptor protein, the most well-characterised of which is the PDZ domain-containing sorting nexin SNX27.

Neuroligins (NLGs) are postsynaptic trans-synaptic scaffold proteins that function in the clustering of postsynaptic proteins to maintain synaptic stability. Here, we show that each of the NLGs (NLG1-3) bind to SNX27 in a direct PDZ ligand-dependent manner. Depletion of SNX27 from neurons leads to a decrease in levels of each NLG protein and, for NLG2, this occurs as a result of enhanced lysosomal degradation. Notably, while depletion of the core retromer component VPS35 leads to a decrease in NLG1 and NLG3 levels, NLG2 is unaffected, suggesting that, for this cargo, SNX27 acts independently of retromer.

Consistent with loss of SNX27 leading to enhanced lysosomal degradation of NLG2, knockdown of SNX27 results in fewer NLG2 clusters in cultured neurons, and loss of SNX27 or VPS35 reduces the size and number of gephyrin clusters. Together, these data indicate that NLGs are SNX27-retromer cargoes and suggest that SNX27-retromer controls inhibitory synapse number, at least in part through trafficking of NLG2.

Keywords: Gephyrin / Inhibitory synapse / Neuroligin / Retromer / SNX27

Abbreviations: AMPA – α-amino-3-hydroxy-5-methyl-4-isoxazolepropionic acid; EGFR – epidermal growth factor receptor; NLG – neuroligin; NMDA – N-methyl-D-aspartate; NRX – neurexin; PDZ – postsynaptic density 95 (PSD95), disk large, zona occludens; SNX – sorting nexin; TGN – *trans*-Golgi network; VPS – vacuolar protein sorting.

Introduction

Retromer is a highly conserved endosomal sorting complex involved in the retrieval and retrograde transport of endocytosed transmembrane proteins (cargoes) to the *trans*-Golgi network (TGN) or cell surface [1, 2]. The core cargo recognition complex of retromer comprises three vacuolar protein sorting (VPS) proteins, VPS26, VPS29 and VPS35 which, in association with multiple other proteins, including members of the sorting nexin (SNX) family [3, 4], concentrate cargoes on the endosomal surface for subsequent sorting. For many cargo proteins, the core retromer complex is sufficient for sequence-specific cargo recognition. Additionally, however, cargoes can be coupled to retromer through adaptor proteins, the best-characterised of which is SNX27.

SNX27 is the only SNX to contain a PDZ domain and binds to type 1 PDZ-binding motifs of interacting proteins [5]. To simultaneously interact with a cargo protein and the retromer complex, the PDZ domain of SNX27 has an extended core fold allowing it to bind VPS26 non-canonically [6]. Through this mechanism, SNX27 links PDZ ligand-containing cargo proteins to the endosomal trafficking machinery, rescuing them from lysosomal degradation and promoting recycling to the plasma membrane [4, 7, 8].

The first validated transmembrane cargo of SNX27-retromer was the β_2-adrenergic receptor [7]. Subsequent proteomics and structural analyses have identified over 400 potential SNX27 transmembrane protein ligands [9, 10], suggesting SNX27 acts as a major sorting determinant for a wide array of cargo proteins. Furthermore, while many of these SNX27 cargoes require retromer for their retrieval, many are insensitive to retromer depletion, suggesting that, for some cargo proteins, SNX27 can promote recycling independently of retromer [10].

The role and cargoes of retromer and SNX27 are of particular interest in neurons because of the highly complex and stringently regulated trafficking of membrane proteins required to maintain neuronal excitability and support synaptic transmission. SNX27-retromer cargoes identified in neurons include AMPA and NMDA-type glutamate receptors, which support the vast majority of excitatory synaptic transmission [11-16] and Kir3 potassium channels [17, 18]. Furthermore, consistent with an important role in neuronal function, SNX27 heterozygous knockout mice have diminished numbers of AMPA and NMDA receptors and exhibit learning and memory deficits [15]. These workers also reported that SNX27 is reduced in human Down's syndrome brains and up-regulating SNX27 rescues defects in Down's syndrome model mice [15]. Moreover, point mutations in the retromer components VPS26 and VPS35 lead to familial Parkinson’s disease [19], and levels of retromer are reduced in the brains of humans with Alzheimer’s disease [20], suggesting that defective retromer-dependent trafficking pathways may directly lead to various neurodegenerative disease states.

While the actions of SNX27-retromer at excitatory synapses is the subject of extensive research, potential roles at inhibitory synapses have been less widely explored. However, a recent proteomics study identified the inhibitory synapse-specific protein neuroligin 2 (NLG2) as a candidate SNX27-retromer cargo [10] and it has subsequently been reported that the core retromer component VPS35 associates with NLG2 in cultured hippocampal neurons [21].

NLGs are postsynaptic cell adhesion molecules that act as ligands for presynaptic neurexins (NRXs) to form trans-synaptic complexes [22, 23]. NLG2 is well established to play key roles in the maturation and function of inhibitory synapses [24, 25]. Importantly, NLG2 interacts with the Rho GDP/GTP-exchange factor collybistin to recruit and cluster the inhibitory postsynaptic scaffolding protein gephyrin [26-28], which is required for the synaptic localisation of glycine receptors (GlyRs) and major $GABA_A$ receptor ($GABA_AR$) subtypes [29, 30]. Correspondingly, mice lacking NLG2 display anxiety phenotypes, have dysfunctional inhibitory postsynaptic structures [31] and show a decrease in both postsynaptic gephyrin and $GABA_AR$ cluster density in hippocampal neurons [32]. Moreover, mutations in NLG2 are implicated in a range of psychiatric disorders including autism spectrum disorder and schizophrenia [33-36].

In this study, we show that SNX27 interacts with each of the NLG proteins, and rescues NLG2 from lysosomal degradation. Moreover, loss of SNX27, or of the core retromer component VPS35, perturbs the clustering of NLG2 and, correspondingly, reduces inhibitory synapse number as assessed by staining for the inhibitory synapse marker protein gephyrin. These data highlight SNX27 as a novel regulator of NLG trafficking, and SNX27-retromer as an important determinant of inhibitory synapse number, at least in part, through regulation of NLG2.

Methods

Antibodies

The following antibodies were used in this study: anti-β-Actin (mouse monoclonal, Sigma-Aldrich, clone AC-15, A5441, 1:10,000), Anti-EGFR (rabbit monoclonal, Abcam, ab52894, 1:1000), Anti-Gephyrin (mouse monoclonal, Synaptic Systems, clone mAb7a, 147 021, 1:1000) Anti-GFP (chicken polyclonal, Abcam, ab13970, 1:600), Anti-GFP (rat monoclonal, ChromoTek, 3H9, 1:5000), Anti-GluA2 (rabbit polyclonal, Synaptic Systems, 182 103, 1:1000), Anti-GST (goat polyclonal, GE Healthcare, 27-4577-01, 1:10,000), Anti-HA (mouse monoclonal, Sigma-Aldrich, clone HA-7, H3663, 1:1000), Anti-HA (rabbit polyclonal, Sigma Aldrich, H6908, 1:100), Anti-LAMP1 (rabbit polyclonal, Abcam, ab24170, 1:1000), Anti-NLG1 (mouse monoclonal, Neuromab, N97A/31, 1:500), Anti-NLG2 (mouse monoclonal, Synaptic

Systems, clone 5E6, 129 511, 1:2000 WB, 1:600 ICC), Anti-NLG3 (mouse monoclonal, Neuromab, N110/29, 1:500), Anti-GluN1 (rabbit monoclonal, Cell Signaling, D65B7 5704, 1:2000), Anti-SNX27 (mouse monoclonal, Abcam, clone 1C6, ab77799, 1:1000), Anti-SNX27 (rabbit polyclonal, a kind gift from Dr Martin Playford (NIH, USA), 1:2000), Anti-VPS35 (rabbit polyclonal, Abcam, ab97545, 1:2000).

DNA constructs and shRNA

For Sindbis virus production, human SNX27 was cloned into the vector pSinRep5(nsP2S) [37]. The intracellular CT of NLG1 (amino acids 719 – 843), NLG2 (amino acids 700 – 836) and NLG3 (amino acids 731 – 848) were cloned from rat whole brain cDNA into the vector pEGFP-C3. The PDZ-AAA mutants of NLG CT were created by site-directed mutagenesis of the NLG1-3 CT pEGFP-C3 constructs. For the purification of recombinant protein, human SNX27 was subcloned into the vector pET28a and rat NLG2-CT-WT and –PDZ-AAA into pGEX-4T-1. For lentivirus production, shRNAs driven by an H1 promoter were produced for the knockdown of rat SNX27 (target sequence 5'-aagaacagcaccacagaccaa-3'), rat VPS35 (target sequence 5'- aacagtggagatattcaataa-3' [38]) and rat NLG2 (target sequence 5'-gcaagttcaacagcaaggaaa-3') and oligonucleotides were cloned into a modified pXLG3-GFP viral vector [39]. To ensure specificity, shRNA target sequences were BLAST searched against the rat genome before use. For rescue experiments, GFP-tagged rat SNX27 or VPS35 were silently point-mutated at 3 consecutive codons in the shRNA target sequence to make them insensitive to the shRNA, and cloned into the corresponding shRNA construct in place of GFP. The fidelity of all constructs was confirmed by DNA sequencing.

Cell culture and transfection

Primary neuronal cultures were prepared from embryonic day (E) 18 Wistar rat brains. Dissociated cortical cells were grown in 35 mm plastic dishes ($5.5x10^5$ cells per well) and hippocampal cells were grown on 25 mm glass coverslips ($1.6x10^5$ cells per coverslip) in plating medium (Neurobasal medium, 5% horse serum, 2 % B27, 1 % Glutamax), which was exchanged for feeding medium 16 hours after plating (Neurobasal medium, 2 % B27, 0.4% Glutamax). HEK293T cells were cultured in a T75 flask containing Complete DMEM medium (DMEM medium, 10 % Fetal Bovine Serum, 1 % L-glutamine and 1 % Penicillin/Streptomycin) and regularly passaged. For transfection, HEK293T cells were grown in 35 mm plastic dishes in Complete DMEM medium which was replaced prior to transfection with Transfection DMEM medium (DMEM medium, 10 % FBS and 1 % L-glutamine). All cells were cultured in a humidified incubator at 37 °C and 5 % CO_2. Hippocampal neurons (for all imaging experiments) and HEK293T cells were transfected using Lipofectamine 2000 (Thermo Fisher).

Lentivirus and Sindbis virus production

Lentiviruses were produced in HEK293T cells by transfection of pXLG3 virus constructs along with the helper vectors pMD2.G and p8.91, as described previously [40]. Sindbis viruses were produced in BHK cells as described previously [41].

Cell lysing and immunoprecipitation

All solutions were pre-chilled to 4 °C and all steps were carried out on ice. Cells were washed with 1x PBS and lysed in lysis buffer (50mM Tris pH 7.4, 150mM NaCl, 0.5 % Triton X-100 and cOmplete protease inhibitors (Roche) in ddH_2O). Lysates were briefly vortexed, kept on ice for 20 min to allow for protein solubilisation and then clarified by centrifuging at 20,000 *g* for 20 min at 4 °C. Lysate supernatants were either used for Western blotting or for immunoprecipitation in which case a 25 µl input sample was retained. GFP-trap beads (ChromoTek) were washed twice with lysis buffer by centrifuging at 1000 *g* for 2 min at 4 °C. Lysate was then added to the beads and incubated for 1 hour at 4 °C after which the beads were washed three times with lysis buffer. Samples were prepared for Western blotting by being resuspended in 2x Laemmli sample buffer and boiled for 5 min at 95 °C.

Surface biotinylation

Surface biotinylation experiments were carried out as described previously [42]. Briefly, neurons were washed in ice-cold PBS, followed by labelling with 0.3 mg/ml Sulfo-NHS-SS-Biotin (Thermo Fisher). After extensive washes with PBS, and a single wash with 50 mM ammonium chloride to quench any unreacted biotin, cells were lysed and cleared lysates prepared as described above. A lysate sample was then taken, and equal amounts of lysate were incubated with streptavidin-agarose (Sigma Aldrich) on a wheel for 1 hour at 4 °C. Beads were then washed 4 times with lysis buffer, and proteins eluted by heating in 2x Laemmli buffer for 10 minutes at 95 °C.

Western blotting

Samples for Western blotting were resolved by sodium dodecyl sulphate-polyacrylamide gel electrophoresis (SDS-PAGE) and separated proteins were transferred to Immobilon-PVDF (polyvinylidene difluoride) 0.45 µm membrane (Merck Millipore). After protein transfer, the membrane was briefly washed with TBS-T (1x Tris Buffered Saline, 0.1 % Tween), blocked in 5 % non-fat milk powder and incubated with primary antibody diluted in 5 % non-fat milk powder for 1 hour at RT. Following incubation, the membrane was briefly washed three times with TBS-T and incubated with HRP-conjugated secondary antibody (Sigma-Aldrich, 1:10,000) diluted in 5 % non-fat milk powder for 45 min at RT. Afterwards, the membrane was washed three times for 5 min in TBS-T at RT and incubated for 1 min at RT with Enhanced Chemiluminescence (ECL) substrate. Protein bands were visualised using an Odyssey Fc (LI-

COR) detection system or in a dark room by exposing X-ray film (Kodak) to the membrane and developing the film with an automatic medical X-ray film processor (Konica).

Recombinant protein purification and *in vitro* interaction assay

SNX27 in the vector pET28a and NLG2-CT-WT and –PDZ-AAA in pGEX-4T-1 were transformed into competent BL21 *Escherichia coli* (*E. coli*) using standard procedures. Single colonies were grown in ampicillin-containing 2xYT broth at 37 °C and protein production was induced with 25 µM isopropyl β-D-thiogalactopyranoside (IPTG) for 15 h at 18 °C. *E. coli* were then centrifuged at 3000 *g* for 20 min at 4 °C to pellet cells and resuspended in lysis buffer (25 mM Tris pH 7.5, 150 mM NaCl, 10 % glycerol and cOmplete protease inhibitors in ddH_2O + 10 mM imidazole for His-fusion protein only) and supplemented with Triton X-100 to a final concentration of 1 %. Cells were lysed by sonication, left on ice for 15 min to allow for solubilisation and clarified by centrifugation at 50,000 *g* for 30 min at 4 °C. Glutathione or Ni-NTA Sepharose 4 Fast Flow beads were washed twice with wash buffer (25 mM Tris pH 7.5, 150 mM NaCl, 10 % glycerol and 1 % Triton X-100 in ddH_2O) and bacterial lysate was incubated on washed beads for 2 h at 4 °C. Following incubation, the beads were washed four times with wash buffer and fusion proteins were eluted with three 5 min incubations at RT with elution buffer (wash buffer supplemented with 10 mM glutathione for GST-fusion proteins or wash buffer without glycerol and Triton X-100 supplemented with 250 mM imidazole for His-fusion protein). To test for interactions, Glutathione Sepharose 4 Fast Flow beads were washed twice with bead wash buffer (50 mM Tris pH 7.4, 150 mM NaCl, 1 % Triton X-100 and cOmplete protease inhibitors in ddH_2O).1 µg GST or GST-NLG2 CT in binding buffer (wash buffer containing 0.1 % BSA) was incubated with the washed beads for 1 h at 4 °C. Following immobilisation, beads were washed four times with bead wash buffer, then incubated with 50 ng His-SNX27 in binding buffer for 2 h at 4 °C and subsequently washed three times with bead wash buffer. 8 ng His-SNX27 in binding buffer was used as an input and all samples were prepared for Western blotting by resuspension in 2x Leammli sample buffer and boiled for 5 min at 95 °C.

Immunocytochemistry

Hippocampal neurons on glass coverslips were transfected with DNA constructs on DIV 16 and fixed and immunostained for confocal microscopy on DIV 21. Neurons were fixed in warm 4 % PFA (paraformaldehyde) in 1x PBS (phosphate-buffered saline) for 15 min and then washed three times with 1x PBS. The PFA was quenched with 1 ml 100mM glycine in 1x PBS after which the neurons were washed three times with 1x PBS. Neurons were then permeabilised and blocked with TBP (0.1 % Triton X-100 and 2 % Bovine Serum Albumin (BSA) in 1x PBS) for 20 min. After blocking, the neurons were incubated with primary

antibodies diluted in 3 % BSA in 1x PBS for 45 min and washed three times with 1x PBS. The neurons were then incubated with Cy2-, Cy3- or Cy5-conjugated secondary antibodies (Sigma-Aldrich, 1:600) diluted in 3 % BSA in 1x PBS for 45 min. After four washes with 1x PBS the coverslips were mounted on glass microscope slides using Fluoromount-G with DAPI (Thermo Fisher) and stored at 4 °C until imaged.

Image acquisition and quantification

Confocal images were captured using a 63x HCX PL APO CS oil-immersion objective on a Leica SP5-II confocal laser scanning microscope attached to a Leica DMI 6000 inverted epifluorescence microscope. All parameters, including excitation and gain, were kept constant across all neurons and coverslips imaged in an experiment to generate a complete data set. A full data set was acquired by imaging eight neurons from three different coverslips from three independent dissections per experimental group unless otherwise stated. Image analysis was performed using ImageJ software (NIH) in combination with the Fiji image processing package. For each neuron, the Z-stack was projected at maximum intensity and three regions of interest (ROI) were drawn free-hand around secondary dendrites. For cluster analysis, the channel was thresholded to create a binary image and the cluster size (area in μm^2) and density per ROI were measured using the Analyse Particles Tool. For quantification of colocalisation, the Pearson's correlation for each ROI was measured using the Colocalisation coloc2 Tool. Numerical values obtained in ImageJ were processed in Microsoft Excel and exported to Graphpad Prism (version 7.0) for statistical analysis.

Statistical analysis

For statistical analysis of cluster size, a cumulative frequency distribution analysis showed a non-parametric distribution and values were therefore compared for statistical significance using a Kolmogorov-Smirnov or Kruskal-Wallis test. Statistical analysis of cluster density and Pearson's correlation were performed using a Student *t*-test or ANOVA. Statistical analysis of Western blots was performed using one-sample *t*-test followed by Bonferroni *post-hoc* test to account for multiple comparisons. Data are presented as ± SEM and parameters for significance are *p<0.05, **p<0.01, ***p<0.001 and ****p<0.0001.

Results

SNX27 interacts with NLG1, 2 and 3

We first investigated if SNX27 binds to NLGs by expressing GFP-SNX27 in cultured cortical neurons using Sindbis virus. Neurons were infected with virus at DIV 17, and GFP-SNX27

interacting proteins were isolated by GFP-trap assays 20-22h post-infection, followed by Western blotting for NLG1, 2 and 3. As shown in Fig 1A all of the endogenous NLG subtypes co-immunoprecipitated with GFP-SNX27. To determine whether this interaction was mediated by the intracellular C-terminal (CT) domains of the NLGs, we next expressed the CT domains of each NLG fused to GFP in HEK293T cells, and isolated interacting proteins by GFP-trap followed by Western blotting for endogenous SNX27 (Fig 1B). Again NLG1-3 CT interacted with SNX27, but the affinity for SNX27 was highest in the case of NLG2.

To define if NLG binding to SNX27 was mediated by PDZ interactions we mutated the C-terminal PDZ-ligand in the GFP-NLG1-3 CT constructs (Threonine^{-2}, Arginine^{-1}, Valine^{0}) to three Alanines and expressed these GFP-tagged PDZ-AAA mutants in HEK293T cells. In all cases, the SNX27-NLG interaction was completely lost in the GFP-NLG-CT-PDZ-AAA mutants (Fig 1C), consistent with NLG1-3 interacting with SNX27 through their C-terminal PDZ ligands.

SNX27 binding to NLG2 is directly mediated by a type 1 PDZ interaction

Given that NLG2 bound most robustly to SNX27 in our assays, and the fact that it is a key component of inhibitory synapses, we focused the properties and potential roles of SNX27-retromer interaction with NLG2. To exclude any contribution of an indirect association and confirm that NLG2 and SNX27 bind directly via a PDZ interaction, we performed *in vitro* binding assays using purified proteins. Free GST, GST-NLG2-CT-WT, GST-NLG2-CT-PDZ-AAA and His-SNX27 were expressed and purified from *E. coli*. The purified GST fusion proteins were incubated with His-SNX27 and isolated on glutathione beads followed by Western blotting. As shown in Fig 2, recombinant His-SNX27 bound to GST-NLG2-CT-WT but not to GST-NLG2-CT-PDZ-AAA, confirming a direct PDZ-mediated interaction between SNX27 and NLG2.

SNX27 knockdown decreases total levels of NLG1-3 and known synaptic SNX27-retromer cargoes

Knockdown of SNX27, or of the core retromer component VPS35, decreases total levels of cargo proteins in clonal cell lines by preventing their retrieval from lysosomal degradation [10]. We therefore examined the effects of knocking down SNX27 or VPS35 in cultured rat cortical neurons. Neurons were infected at DIV 9-11 with lentiviral constructs that express shRNAs against SNX27 (shSNX27), VPS35 (shVPS35) or a control non-targeting shRNA. Seven days post-infection, neurons were lysed and protein levels analysed by Western blotting. shSNX27 and shVPS35 were very efficient and significantly decreased levels of SNX27 and VPS35 to 13.1±3.26% and 15.6±3.49%, respectively, of control cells (Fig 3A, and C).

Consistent with SNX27 playing a key role in NLG recycling, SNX27 knockdown dramatically reduced levels of NLG1-3, indicating that these proteins are rescued from degradation in a manner dependent on their interaction with SNX27 (Fig 3B and D). In addition, we tested the levels of subunits of AMPARs and NMDARs, which have both been previously reported as SNX27-retromer cargoes [11, 13-16]. Consistently, shSNX27 significantly reduced total levels of the AMPAR subunit GluA2 and NMDAR subunit GluN1. Total levels of EGFR, which is not a retromer cargo [10], were unaffected by SNX27 or VPS35 knockdown (Fig 3B and E). Importantly, the reduced levels of NLG2 following SNX27 knockdown were rescued to control levels by concomitant re-expression of a GFP-tagged shRNA-resistant SNX27 (Supplementary Fig 1A), confirming the effects of the knockdown were specific to loss of SNX27.

SNX27 traffics NLG2 independently of retromer

Interestingly, knockdown of the core retromer component VPS35 had a different profile to SNX27 knockdown. NLG1 and NLG3 levels were significantly reduced by shVPS35, albeit not to the same extent as for shSNX27, suggesting their trafficking is partly dependent on the core retromer trimer (Fig 3B and D). Levels of GluA2 were also reduced to a similar extent by shSNX27 and shVPS35. Again, we validated the specificity of these effects by confirming that the loss of NLG1 and NLG3 upon VPS35 knockdown was rescued by expression of a GFP-tagged shRNA-resistant VPS35 (Supplementary Fig 1B).

In stark contrast, however, total levels of NLG2 and of the NMDAR subunit GluN1, which were reduced by >50% by shSNX27, were unaffected by shVPS35. Intriguingly, these results suggest that SNX27 selectively acts via a mechanism independent of the core retromer VPS trimer in the recycling of NLG2 and GluN1 (Fig 3B and E).

SNX27 knockdown reduces NLG2 surface expression

To determine whether the loss of total NLG2 resulting from SNX27 knockdown also led to a corresponding loss of NLG2 from the cell surface, we performed surface biotinylation experiments. Neurons were infected with control, shSNX27 or shVPS35 viruses at DIV 9-11 and surface proteins labelled with biotin 7 days later. Cells were then lysed, and surface proteins isolated on streptavidin beads. SNX27 knockdown decreased total NLG2 levels with a corresponding decrease in surface NLG2 levels (Supplementary Fig 2). VPS35 knockdown, on the other hand, did not alter either total NLG2 or surface NLG2 levels (Supplementary Fig 2).

SNX27 knockdown increases lysosomal degradation of NLG2

To investigate the mechanism underlying SNX27 regulation of total NLG2 levels we analysed colocalisation of NLG2 with the lysosomal marker protein LAMP1 following SNX27 or VPS35 knockdown. Neurons were transfected with shRNA constructs at DIV 16 and then fixed and stained for NLG2 and LAMP1 5 days later. As expected from knockdown of SNX27 leading to a loss of total NLG2 protein, shSNX27 resulted in a significant increase in NLG2/LAMP1 colocalisation (Fig 4A and B). However, consistent with the lack of effect of VPS35 knockdown on NLG2 (Fig 3B and D), shVPS35 did not increase NLG2/LAMP1 colocalisation (Fig 4A and B). Importantly, knockdown of SNX27 or VPS35 had no effect on LAMP1 cluster density or cluster size (Supplementary Fig 3), indicating loss of these proteins was not altering global levels of lysosomal degradation. These data indicate that SNX27, but not VPS35 retromer, is involved in retrieving NLG2 from lysosomal degradation.

SNX27 knockdown decreases the density but not the size of NLG2 clusters

NLG2 is predominantly localised at inhibitory synapses so we next investigated how SNX27 or VPS35 knockdown affects NLG2 distribution. DIV 16 hippocampal neurons were transfected with GFP-tagged shSNX27, fixed at DIV 21, and immunostained for gephyrin, a scaffolding protein that is a central component of inhibitory synapses [26], and NLG2, and imaged by confocal microscopy (Fig 5). For these experiments, we chose to analyse NLG2 clusters in secondary dendrites, defined as dendritic branches emerging from primary dendrites which in turn emerge from the soma. This approach allowed us to unambiguously identify single NLG2 clusters away from the high density of clusters around the soma. These analyses revealed a significant decrease in the number of NLG2 puncta in both SNX27 or VPS35 knockdown neurons (Fig 5A and B). Furthermore, there was a significant decrease in the size of NLG2 puncta in the VPS35 knockdown cells. Surprisingly, however, the size of NLG2 puncta was not significantly reduced by SNX27 knockdown (Fig 5A and C).

SNX27 or VPS35 knockdown decrease both the density and size of gephyrin clusters

NLG2 has been reported to recruit and directly bind gephyrin so we next tested the effects of SNX27 or VPS35 knockdown on gephyrin clustering. Consistent with their effects on NLG2, ablation of either SNX27 or VPS35 significantly decreased the size and density of gephyrin clusters in hippocampal neurons, demonstrating that both SNX27 and retromer play key roles in regulating the number of inhibitory synapses (Fig 6).

NLG2 knockdown significantly decreases size and density of gephyrin clusters

Finally, to determine if the effects of SNX27 or VPS35 knockdown on gephyrin clustering are mediated by NLG2, we directly knocked down NLG2. Our shNLG2 caused a ~50% decrease in NLG2 levels (Fig 7A and B), similar to the effect of shSNX27 on total NLG2 levels (Fig 3). Interestingly, ~50 loss of NLG2, directly mimicking the effect of SNX27 loss, resulted in a

reduction in the density and size of gephyrin clusters, similar to loss of SNX27 or VPS35 (Fig 7C, D and E). Taken together, our data are consistent with a model whereby loss of SNX27 or VPS35 affects inhibitory synapse number via altered stability or clustering of NLG2, and highlight SNX27 and retromer as novel determinants of inhibitory synapse number, at least in part, through regulation of NLG2.

Discussion

It is well established that the regulation and trafficking of NLGs is an important determinant of synapse formation and stability [22, 23]. However, relatively little is known about how NLG trafficking is mediated, and few direct NLG interacting proteins have been identified.

Here we identify NLG1-3 as novel SNX27 PDZ binding proteins and show that loss of SNX27 in cultured neurons decreases NLG1-3 levels. Since NLG2, a NLG primarily involved in the maintenance of inhibitory synapses [26-28], was the highest affinity SNX27 interactor, we focused on this interaction. We show that loss of SNX27 increases lysosomal degradation of NLG2 and reduces the number of NLG2 clusters in cultured hippocampal neurons. These data demonstrate that SNX27 plays a key role in rescuing endocytosed NLG2 from lysosomal degradation to allow recycling back to the plasma membrane.

Interestingly, knockdown of the core retromer component VPS35 neither decreased total levels of NLG2 nor increased localisation at lysosomes. However, VPS35 knockdown did decrease both NLG2 cluster size and density in secondary dendrites. The most straightforward explanation for these results is that increased degradation of another, as yet unidentified, retromer cargo plays a role in NLG2 clustering. Indeed, it has been reported that NLG2 can heterodimerise with NLG3 at inhibitory synapses [43]. Since NLG3 levels were reduced by VPS35 knockdown, it remains possible that loss of VPS35 results in reduced NLG2 clustering through loss of NLG3. Nonetheless, together with knockdown of SNX27, these data indicate that both SNX27 and VPS35 control the number or size of NLG2 clusters through either direct trafficking of NLG2 (via SNX27) and indirect mechanisms (VPS35).

It is notable that, while knockdown of SNX27 reduced levels of all NLG proteins, knockdown of VPS35 did not reduce total levels of NLG2, and reduced levels of NLG1 and NLG3 more modestly than knockdown of SNX27. Thus, SNX27 appears to retrieve NLG2 from degradation in a manner distinct from its more well-characterised role of acting as a PDZ adaptor protein for retromer. While the mechanisms underpinning this retromer-independent trafficking pathway remain to be defined, we observed a similar profile for the NMDA receptor subunit GluN1, suggesting it may represent an important additional regulatory pathway for

synaptic membrane proteins. Indeed, a previous proteomic study identified proteins in HeLa cells that are reduced or lost following knockdown of SNX27 but not of VPS35, suggesting this may represent a generalised SNX27-dependent trafficking pathway [10].

NLG2 plays a key role in regulating inhibitory synapse number through controlling the clustering of the postsynaptic scaffold protein gephyrin [26] but there have been no reports for the involvement of SNX27-retromer in this process. Here, consistent with the effects of knockdown of SNX27 or VPS35 on NLG2 cluster size and density, we show that knockdown of SNX27 or VPS35 reduced gephyrin cluster size and density and thus inhibitory synapse number. Moreover, these effects on gephyrin clustering are similar to directly knocking down NLG2, suggesting that the effects of SNX27 or VPS35 on inhibitory synapse number are mediated, at least in part, through controlling the abundance and targeting of NLG2.

SNX27 dysfunction has been shown to underlie excitatory synaptic defects associated with Down's Syndrome and epilepsy [15, 44]. Moreover, retromer dysfunction has been reported in a number of neurodegenerative disorders, including Alzheimer's and Parkinson's diseases [19, 20, 45]. Our results indicate that retromer and/or SNX27 dysfunction likely contribute to pathogenesis through altered degradation or mistargeting of the NLG proteins. In particular, our data demonstrate that SNX27 and retromer control inhibitory synapse number, at least in part through trafficking of NLG2, suggesting that retromer dysfunction could play a role in disorders characterised by aberrant inhibitory synaptic transmission or network function, such as epilepsy and autism. Further studies will be required to investigate this exciting possibility.

Acknowledgements:

We thank Dr Martin Playford (NIH, USA) for the generous gift of the rabbit SNX27 antibody used in this study, and Dr Kirsty McMillan for critical reading of the manuscript. We also thank the Wolfson Bioimaging Facility (University of Bristol).

Funding Information:

We are grateful to the MRC (K.A.W and J.M.H), BBSRC (K.A.W and J.M.H), Parkinson's UK (K.A.W and J.M.H), Alzheimer's Research UK (K.A.W) and British Heart Foundation (J.M.H) for funding. C.S.B. was funded by a BRACE PhD studentship.

Author Contributions:

C.S.B. performed all imaging, and the majority of biochemistry and molecular biology. Y.N performed VPS35 rescue experiments. J.M.H provided supervision, mentoring and project direction. K.A.W. conceived the project, performed molecular biology and biochemistry, and supervised the project. All authors provided intellectual input into project direction and contributed to writing the manuscript.

Conflict of Interests:

The authors declare that they have no conflict of interest.

Ethics Statement:

All experiments in this study were performed in accordance with UK Home Office Schedule 1 guidelines. Animals were sacrificed by cervical dislocation using procedures approved by the Home Office Licensing Team at the University of Bristol (UIN UB/18/004).

References:

1 Seaman, M. N. (2012) The retromer complex - endosomal protein recycling and beyond. Journal of cell science. **125**, 4693-4702

2 Burd, C. and Cullen, P. J. (2014) Retromer: a master conductor of endosome sorting. Cold Spring Harbor perspectives in biology. **6**

3 Gallon, M. and Cullen, P. J. (2015) Retromer and sorting nexins in endosomal sorting. Biochemical Society transactions. **43**, 33-47

4 Cullen, P. J. and Korswagen, H. C. (2011) Sorting nexins provide diversity for retromer-dependent trafficking events. Nature cell biology. **14**, 29-37

5 Kim, E. and Sheng, M. (2004) PDZ domain proteins of synapses. Nature reviews. Neuroscience. **5**, 771-781

6 Gallon, M., Clairfeuille, T., Steinberg, F., Mas, C., Ghai, R., Sessions, R. B., Teasdale, R. D., Collins, B. M. and Cullen, P. J. (2014) A unique PDZ domain and arrestin-like fold interaction reveals mechanistic details of endocytic recycling by SNX27-retromer. Proceedings of the National Academy of Sciences of the United States of America. **111**, E3604-3613

7 Lauffer, B. E., Melero, C., Temkin, P., Lei, C., Hong, W., Kortemme, T. and von Zastrow, M. (2010) SNX27 mediates PDZ-directed sorting from endosomes to the plasma membrane. The Journal of cell biology. **190**, 565-574

8 Temkin, P., Lauffer, B., Jager, S., Cimermancic, P., Krogan, N. J. and von Zastrow, M. (2011) SNX27 mediates retromer tubule entry and endosome-to-plasma membrane trafficking of signalling receptors. Nature cell biology. **13**, 715-721

9 Clairfeuille, T., Mas, C., Chan, A. S., Yang, Z., Tello-Lafoz, M., Chandra, M., Widagdo, J., Kerr, M. C., Paul, B., Merida, I., Teasdale, R. D., Pavlos, N. J., Anggono, V. and Collins, B. M. (2016) A molecular code for endosomal recycling of phosphorylated cargos by the SNX27-retromer complex. Nature structural & molecular biology. **23**, 921-932

10 Steinberg, F., Gallon, M., Winfield, M., Thomas, E. C., Bell, A. J., Heesom, K. J., Tavare, J. M. and Cullen, P. J. (2013) A global analysis of SNX27-retromer assembly and cargo specificity reveals a function in glucose and metal ion transport. Nature cell biology. **15**, 461-471

11 Temkin, P., Morishita, W., Goswami, D., Arendt, K., Chen, L. and Malenka, R. (2017) The Retromer Supports AMPA Receptor Trafficking During LTP. Neuron. **94**, 74-82 e75

12 Choy, R. W., Park, M., Temkin, P., Herring, B. E., Marley, A., Nicoll, R. A. and von Zastrow, M. (2014) Retromer mediates a discrete route of local membrane delivery to dendrites. Neuron. **82**, 55-62

13 Hussain, N. K., Diering, G. H., Sole, J., Anggono, V. and Huganir, R. L. (2014) Sorting Nexin 27 regulates basal and activity-dependent trafficking of AMPARs. Proceedings of the National Academy of Sciences of the United States of America. **111**, 11840-11845

14 Loo, L. S., Tang, N., Al-Haddawi, M., Dawe, G. S. and Hong, W. (2014) A role for sorting nexin 27 in AMPA receptor trafficking. Nature communications. **5**, 3176

15 Wang, X., Zhao, Y., Zhang, X., Badie, H., Zhou, Y., Mu, Y., Loo, L. S., Cai, L., Thompson, R. C., Yang, B., Chen, Y., Johnson, P. F., Wu, C., Bu, G., Mobley, W. C., Zhang, D., Gage, F. H., Ranscht, B., Zhang, Y. W., Lipton, S. A., Hong, W. and Xu, H. (2013) Loss of sorting nexin 27 contributes to excitatory synaptic dysfunction by modulating glutamate receptor recycling in Down's syndrome. Nature medicine. **19**, 473-480

16 Cai, L., Loo, L. S., Atlashkin, V., Hanson, B. J. and Hong, W. (2011) Deficiency of sorting nexin 27 (SNX27) leads to growth retardation and elevated levels of N-methyl-D-aspartate receptor 2C (NR2C). Molecular and cellular biology. **31**, 1734-1747

17 Lunn, M. L., Nassirpour, R., Arrabit, C., Tan, J., McLeod, I., Arias, C. M., Sawchenko, P. E., Yates, J. R., 3rd and Slesinger, P. A. (2007) A unique sorting nexin regulates trafficking of potassium channels via a PDZ domain interaction. Nature neuroscience. **10**, 1249-1259

18 Balana, B., Maslennikov, I., Kwiatkowski, W., Stern, K. M., Bahima, L., Choe, S. and Slesinger, P. A. (2011) Mechanism underlying selective regulation of G protein-gated inwardly

rectifying potassium channels by the psychostimulant-sensitive sorting nexin 27. Proceedings of the National Academy of Sciences of the United States of America. **108**, 5831-5836
19 McMillan, K. J., Korswagen, H. C. and Cullen, P. J. (2017) The emerging role of retromer in neuroprotection. Current opinion in cell biology. **47**, 72-82
20 Small, S. A., Kent, K., Pierce, A., Leung, C., Kang, M. S., Okada, H., Honig, L., Vonsattel, J. P. and Kim, T. W. (2005) Model-guided microarray implicates the retromer complex in Alzheimer's disease. Annals of neurology. **58**, 909-919
21 Kang, Y., Ge, Y., Cassidy, R. M., Lam, V., Luo, L., Moon, K. M., Lewis, R., Molday, R. S., Wong, R. O., Foster, L. J. and Craig, A. M. (2014) A combined transgenic proteomic analysis and regulated trafficking of neuroligin-2. The Journal of biological chemistry. **289**, 29350-29364
22 Sudhof, T. C. (2008) Neuroligins and neurexins link synaptic function to cognitive disease. Nature. **455**, 903-911
23 Bemben, M. A., Shipman, S. L., Nicoll, R. A. and Roche, K. W. (2015) The cellular and molecular landscape of neuroligins. Trends in neurosciences. **38**, 496-505
24 Graf, E. R., Zhang, X., Jin, S. X., Linhoff, M. W. and Craig, A. M. (2004) Neurexins induce differentiation of GABA and glutamate postsynaptic specializations via neuroligins. Cell. **119**, 1013-1026
25 Varoqueaux, F., Jamain, S. and Brose, N. (2004) Neuroligin 2 is exclusively localized to inhibitory synapses. European journal of cell biology. **83**, 449-456
26 Poulopoulos, A., Aramuni, G., Meyer, G., Soykan, T., Hoon, M., Papadopoulos, T., Zhang, M., Paarmann, I., Fuchs, C., Harvey, K., Jedlicka, P., Schwarzacher, S. W., Betz, H., Harvey, R. J., Brose, N., Zhang, W. and Varoqueaux, F. (2009) Neuroligin 2 drives postsynaptic assembly at perisomatic inhibitory synapses through gephyrin and collybistin. Neuron. **63**, 628-642
27 Hoon, M., Bauer, G., Fritschy, J. M., Moser, T., Falkenburger, B. H. and Varoqueaux, F. (2009) Neuroligin 2 controls the maturation of GABAergic synapses and information processing in the retina. The Journal of neuroscience : the official journal of the Society for Neuroscience. **29**, 8039-8050
28 Soykan, T., Schneeberger, D., Tria, G., Buechner, C., Bader, N., Svergun, D., Tessmer, I., Poulopoulos, A., Papadopoulos, T., Varoqueaux, F., Schindelin, H. and Brose, N. (2014) A conformational switch in collybistin determines the differentiation of inhibitory postsynapses. The EMBO journal. **33**, 2113-2133
29 Kneussel, M. and Betz, H. (2000) Clustering of inhibitory neurotransmitter receptors at developing postsynaptic sites: the membrane activation model. Trends in neurosciences. **23**, 429-435
30 Moss, S. J. and Smart, T. G. (2001) Constructing inhibitory synapses. Nature reviews. Neuroscience. **2**, 240-250
31 Babaev, O., Botta, P., Meyer, E., Muller, C., Ehrenreich, H., Brose, N., Luthi, A. and Krueger-Burg, D. (2016) Neuroligin 2 deletion alters inhibitory synapse function and anxiety-associated neuronal activation in the amygdala. Neuropharmacology. **100**, 56-65
32 Jedlicka, P., Hoon, M., Papadopoulos, T., Vlachos, A., Winkels, R., Poulopoulos, A., Betz, H., Deller, T., Brose, N., Varoqueaux, F. and Schwarzacher, S. W. (2011) Increased dentate gyrus excitability in neuroligin-2-deficient mice in vivo. Cerebral cortex. **21**, 357-367
33 Blundell, J., Tabuchi, K., Bolliger, M. F., Blaiss, C. A., Brose, N., Liu, X., Sudhof, T. C. and Powell, C. M. (2009) Increased anxiety-like behavior in mice lacking the inhibitory synapse cell adhesion molecule neuroligin 2. Genes, brain, and behavior. **8**, 114-126
34 Sun, C., Cheng, M. C., Qin, R., Liao, D. L., Chen, T. T., Koong, F. J., Chen, G. and Chen, C. H. (2011) Identification and functional characterization of rare mutations of the neuroligin-2 gene (NLGN2) associated with schizophrenia. Human molecular genetics. **20**, 3042-3051
35 Wohr, M., Silverman, J. L., Scattoni, M. L., Turner, S. M., Harris, M. J., Saxena, R. and Crawley, J. N. (2013) Developmental delays and reduced pup ultrasonic vocalizations but normal sociability in mice lacking the postsynaptic cell adhesion protein neuroligin2. Behavioural brain research. **251**, 50-64

36 Mackowiak, M., Mordalska, P. and Wedzony, K. (2014) Neuroligins, synapse balance and neuropsychiatric disorders. Pharmacological reports : PR. **66**, 830-835
37 Kim, J., Dittgen, T., Nimmerjahn, A., Waters, J., Pawlak, V., Helmchen, F., Schlesinger, S., Seeburg, P. H. and Osten, P. (2004) Sindbis vector SINrep(nsP2S726): a tool for rapid heterologous expression with attenuated cytotoxicity in neurons. Journal of neuroscience methods. **133**, 81-90
38 McGarvey, J. C., Xiao, K., Bowman, S. L., Mamonova, T., Zhang, Q., Bisello, A., Sneddon, W. B., Ardura, J. A., Jean-Alphonse, F., Vilardaga, J. P., Puthenveedu, M. A. and Friedman, P. A. (2016) Actin-Sorting Nexin 27 (SNX27)-Retromer Complex Mediates Rapid Parathyroid Hormone Receptor Recycling. The Journal of biological chemistry. **291**, 10986-11002
39 Rocca, D. L., Wilkinson, K. A. and Henley, J. M. (2017) SUMOylation of FOXP1 regulates transcriptional repression via CtBP1 to drive dendritic morphogenesis. Scientific reports. **7**, 877
40 McMillan, K. J., Gallon, M., Jellett, A. P., Clairfeuille, T., Tilley, F. C., McGough, I., Danson, C. M., Heesom, K. J., Wilkinson, K. A., Collins, B. M. and Cullen, P. J. (2016) Atypical parkinsonism-associated retromer mutant alters endosomal sorting of specific cargo proteins. The Journal of cell biology. **214**, 389-399
41 Konopacki, F. A., Jaafari, N., Rocca, D. L., Wilkinson, K. A., Chamberlain, S., Rubin, P., Kantamneni, S., Mellor, J. R. and Henley, J. M. (2011) Agonist-induced PKC phosphorylation regulates GluK2 SUMOylation and kainate receptor endocytosis. Proceedings of the National Academy of Sciences of the United States of America. **108**, 19772-19777
42 Evans, A. J., Gurung, S., Wilkinson, K. A., Stephens, D. J. and Henley, J. M. (2017) Assembly, Secretory Pathway Trafficking, and Surface Delivery of Kainate Receptors Is Regulated by Neuronal Activity. Cell reports. **19**, 2613-2626
43 Budreck, E. C. and Scheiffele, P. (2007) Neuroligin-3 is a neuronal adhesion protein at GABAergic and glutamatergic synapses. The European journal of neuroscience. **26**, 1738-1748
44 Damseh, N., Danson, C. M., Al-Ashhab, M., Abu-Libdeh, B., Gallon, M., Sharma, K., Yaacov, B., Coulthard, E., Caldwell, M. A., Edvardson, S., Cullen, P. J. and Elpeleg, O. (2015) A defect in the retromer accessory protein, SNX27, manifests by infantile myoclonic epilepsy and neurodegeneration. Neurogenetics. **16**, 215-221
45 Small, S. A. and Petsko, G. A. (2015) Retromer in Alzheimer disease, Parkinson disease and other neurological disorders. Nature reviews. Neuroscience. **16**, 126-132

Figure Legends:

Figure 1. SNX27 binds NLG 1-3 through a PDZ-interaction.

(**A**) SNX27 interacts with NLG1-3 in cortical neurons. DIV 14 cortical neurons were infected with a Sindbis virus encoding GFP-SNX27 or GFP. Neurons were lysed 22-24 hours post-infection, subjected to GFP-trap immunoprecipitation and Western blotted as indicated. Note, the bands beneath GFP-SNX27 in the immunoprecipitation likely represent degradation products of the overexpressed GFP-SNX27.

(**B**) The intracellular C-termini (CT) of NLG1-3 bind endogenous SNX27 in HEK293T cells. HEK293T cell were transfected with GFP-NLG1-3 CT. Cells were lysed 48 hours post-transfection, subjected to GFP-trap immunoprecipitation and Western blotted as indicated.

(**C**) Mutation of the NLG PDZ ligands prevent interaction with endogenous SNX27 in HEK293T cells. HEK293T cells were transfected with GFP-NLG1-3 CT WT or PDZ-AAA. Cells were lysed 48 hours post-transfection, subjected to GFP-trap immunoprecipitation and Western blotted as indicated.

Figure 2. SNX27 and NLG 2 bind directly through a PDZ interaction.

(**A**) Bacterially expressed GST-NLG2 CT WT, PDZ-AAA and GST. Coomassie stained gel demonstrating the purity of the proteins used.

(**B**) Bacterially expressed His-SNX27. Coomassie stained gel demonstrating the purity of the protein used.

(**C**) Purified NLG2 CT interacts directly with SNX27 via a PDZ interaction. 1 µg WT and PDZ-AAA GST-NLG2 CT and GST were immobilised on glutathione sepharose beads before being incubated with 50 ng His-SNX27. GST pulldown samples were analysed by Western blotting as indicated.

Figure 3. Loss of SNX27-retromer components decreases total levels of NLGs and of known SNX27-retomer cargoes in cortical neurons.

(**A, B**) Western blots showing total levels of protein expression after SNX27 or VPS35 knockdown. DIV 9-11 cortical neurons were infected with lentiviruses encoding shSNX27, shVPS35 or a control non-targeting shRNA. Neurons were lysed 7 days post-infection and Western blotted as indicated.

(**C, D, E**) Quantification of total levels of protein expression after SNX27 or VPS35 knockdown shown in (A). Data are shown as a percentage of the control (n = 5-7; one sample *t*-test, Bonferroni *post-hoc* test).

Data information: Error bars represent s.e.m. Statistical significance: *P < 0.05; **P < 0.01; ***P < 0.001; ****P < 0.0001.

Figure 4. Knockdown of SNX27 increases lysosomal degradation of NLG2

(**A**) Representative images of NLG2 colocalisation with the lysosomal marker protein LAMP1 in secondary dendrites. DIV 16 hippocampal neurons were transfected with shSNX27, shVPS35 or a non-targeting shRNA. Neurons were fixed, permeabilised and immunostained at DIV 21 for GFP (green), NLG2 (red) and LAMP1 (blue). Arrows highlight areas of colocalisation. Lower panels show enlargement of area indicated by box. Scale bar, 10 μm.

(**B**) Quantification of NLG2 colocalisation with the lysosomal marker protein LAMP1 in secondary dendrites after SNX27 or VPS35 knockdown as shown in (A) using Pearson's correlation (n = 23-24 from 3 independent dissections; One-way ANOVA).

Data information: Error bars represent s.e.m. Statistical significance: *P < 0.05.

Figure 5. Loss of SNX27-retromer function decreases NLG2 cluster size and density in hippocampal neurons.

(**A**) Representative images of NLG2 clusters after SNX27 or VPS35 knockdown. DIV 16 hippocampal neurons were transfected with shSNX27, shVPS35 or a non-targeting shRNA. Neurons were fixed and immunostained at DIV 21 for GFP (green), NLG2 (red) and DAPI (blue). Lower panels show enlargement of area indicated by box. Scale bar, 10 μm.

(**B**) Quantification of NLG2 cluster density per 100 μm^2 of secondary dendrite in hippocampal neurons after SNX27 or VPS35 knockdown as shown in (A) (n = 23-24 from 3 independent dissections; One-way ANOVA).

(**C**) Quantification of NLG2 cluster size in μm^2 in secondary dendrites of hippocampal neurons after SNX27 or VPS35 knockdown as shown in (A) (n = 1552 (shScrambled), 905 (shSNX27) and 854 (shVPS35) from 3 independent dissections; Kruskall-Wallis).

Data information: Error bars represent s.e.m. Statistical significance: **P < 0.01; ***P < 0.001; ****P < 0.0001.

Figure 6. Loss of SNX27-retromer function decreases gephyrin cluster size and density in hippocampal neurons.

(**A**) Representative images of gephyrin clusters after SNX27 or VPS35 knockdown. DIV 16 hippocampal neurons were transfected with shSNX27, shVPS35 or a non-targeting shRNA. Neurons were fixed and immunostained at DIV 21 for GFP (green), gephyrin (red) and DAPI

(blue). Lower panels show enlargement of area indicated by box. Scale bar, 10 μm.

(**B**) Quantification of gephyrin cluster density per 100 μm^2 of secondary dendrite of hippocampal neurons after SNX27 or VPS35 knockdown as shown in (A) (n = 23-24 from 3 independent dissections; One-way ANOVA;).

(**C**) Quantification of gephyrin cluster size in μm^2 in secondary dendrites of hippocampal neurons after SNX27 or VPS35 knockdown as shown in (A) (n = 974 (shScrambled), 301 (shSNX27) and 124 (shVPS35) from 3 independent dissections; Kruskall-Wallis).

Data information: Error bars represent s.e.m. Statistical significance: $^{**}P < 0.01$; $^{****}P < 0.0001$.

Figure 7. NLG2 knockdown decreases gephyrin cluster size and density in hippocampal neurons.

(**A**) Representative images of NLG2 expression after SNX27 or VPS35 knockdown. DIV 16 hippocampal neurons were transfected with shNLG2 or a non-targeting shRNA. Neurons were fixed and immunostained at DIV 21 for GFP (green), NLG2 (red) and DAPI (blue). Lower panels show enlargement of area indicated by box. Scale bar, 10 μm.

(**B**) Quantification of NLG2 expression in secondary dendrites of hippocampal neurons after SNX27 or VPS35 knockdown as shown in (A). Data are presented as a percentage of NLG2 expression in control neurons after transfection with a non-targeting shRNA (n = 8 from 1 independent dissection; Student's *t*-test).

(**C**) Representative images of gephyrin clusters after NLG2 knockdown. DIV 16 hippocampal neurons were transfected with shNLG2 or a non-targeting shRNA. Neurons were fixed and immunostained at DIV 21 for GFP (green), gephyrin (red) and DAPI (blue). Lower panels show enlargement of area indicated by box. Scale bar, 10 μm.

(**D**) Quantification of gephyrin cluster density per 100 μm^2 of secondary dendrite of hippocampal neurons after SNX27 or VPS35 knockdown as shown in (A) (n = 24 from 3 independent dissections; Student's *t*-test).

(**E**) Quantification of gephyrin cluster size in μm^2 in secondary dendrites of hippocampal neurons after NLG2 knockdown as shown in (A) (n = 517 (shScrambled) and 174 (ShNLG2) from 3 independent dissections; Kolmogorov-Smirnov).

Data information: Error bars represent s.e.m. Statistical significance: $^{**}P < 0.01$; $^{***}P < 0.001$; $^{****}P < 0.0001$.

Supplementary Figure 1. The effects of SNX27 or VPS35 loss on NLG levels can be

rescued by re-expression of GFP-SNX27 or GFP-VPS35, respectively.

(**A**) Neurons were infected at DIV 9 with lentiviruses encoding a control shRNA, SNX27 KD or a SNX27 KD virus also expressing shRNA-resistant GFP-SNX27. 7 days later, cells were lysed and subjected to Western blotting as indicated. Quantification of total NLG2 levels, as a percentage of the control, are shown in the graph on the right (n = 4; one sample *t*-test, Bonferroni *post-hoc* test).

(**B**) Neurons were infected at DIV 9 with lentiviruses encoding a control shRNA, VPS35 KD or a VPS35 KD virus also expressing shRNA-resistant GFP-VPS35. 7 days later, cells were lysed and subjected to Western blotting as indicated. Quantification of total NLG1 and NLG3 levels, as a percentage of the control, are shown in the graphs on the right (n = 8; one sample *t*-test, Bonferroni *post-hoc* test).

Data information: Error bars represent s.e.m. Statistical significance: **P* < 0.05; ***P* < 0.01; *****P* < 0.0001.

Supplementary Figure 2. Loss of SNX27 causes a decrease in total NLG2 levels, and a corresponding decrease in surface-expressed NLG2.

(**A**) Neurons were infected at DIV 9-11 with lentiviruses encoding a control shRNA, SNX27 KD or VPS35 KD. 7 days later, surface proteins were labelled with membrane-impermeant biotin prior to cell lysis. Surface proteins were then isolated on streptavidin beads, before being subjected to Western blotting alongside whole lysate samples, as indicated.

(**B**) Quantification of total NLG2 levels from (A), normalized to EGFR to control for protein loading, expressed as percentage of control. (n = 5; one sample *t*-test, Bonferroni *post-hoc* test).

(**C**) Quantification of surface NLG2 levels from (A), normalized to EGFR to control for protein loading, expressed as percentage of control. (n = 5; one sample *t*-test, Bonferroni *post-hoc* test).

Data information: Error bars represent s.e.m. Statistical significance: ***P* < 0.01.

Supplementary Figure 3. Loss of SNX27 or VPS35 has no effect on LAMP1 cluster size or density.

(**A**) LAMP1 cluster size and density in images from Figure 4A were analysed. (n = 23-24 from 3 independent dissections; One-way ANOVA).

Data information: Error bars represent s.e.m.

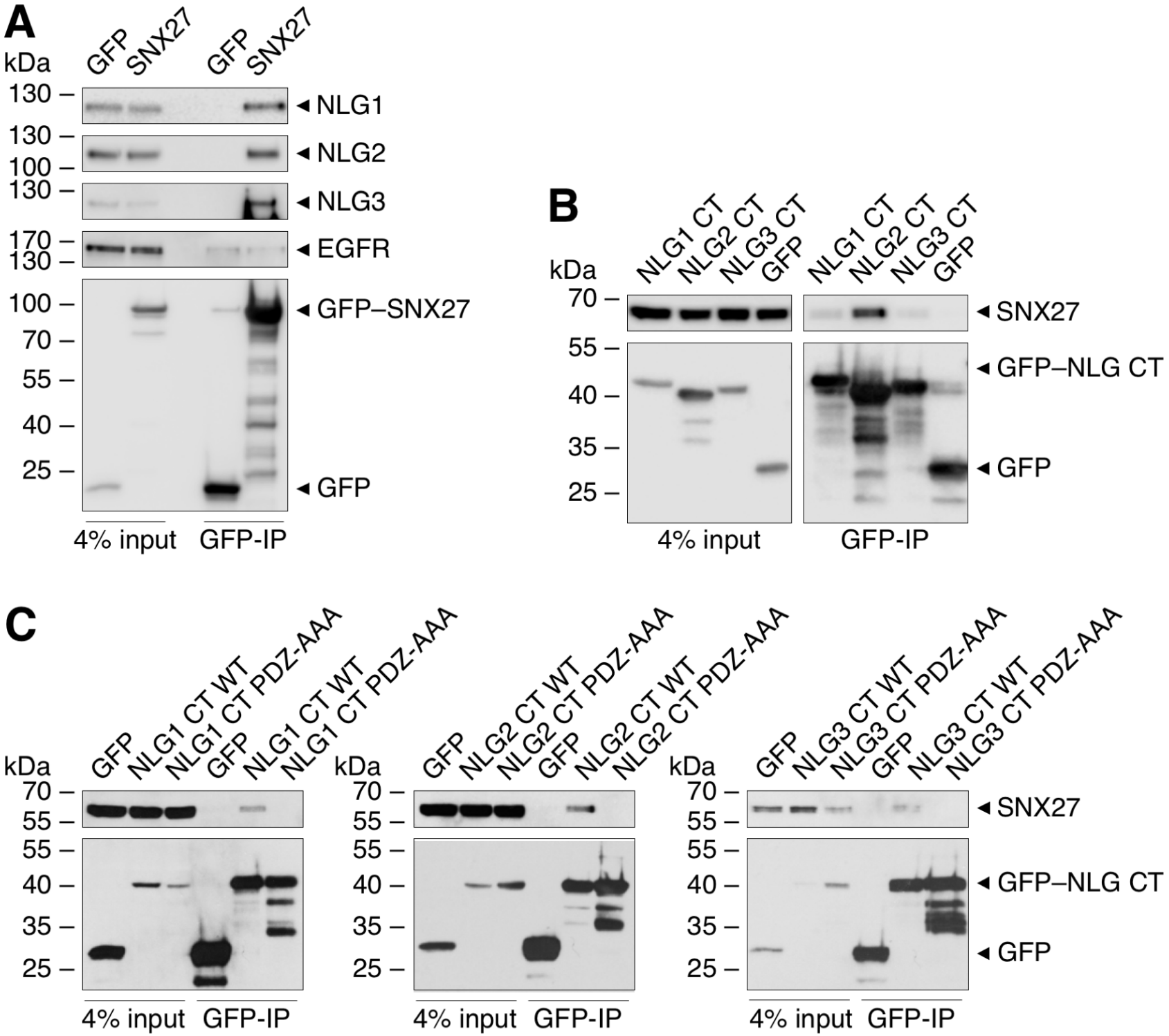
A
kDa
GFP
SNX27
GFP
SNX27
130
130
100
130
170
130
100
70
55
40
25
NLG1
NLG2
NLG3
EGFR
GFP–SNX27
GFP
4% input
GFP-IP
B
kDa
NLG1 CT
NLG2 CT
NLG3 CT
GFP
NLG1 CT
NLG2 CT
NLG3 CT
GFP
70
55
40
35
25
SNX27
GFP–NLG CT
GFP
4% input
GFP-IP
C
kDa
GFP
NLG1 CT WT
NLG1 CT PDZ-AAA
GFP
NLG1 CT WT
NLG1 CT PDZ-AAA
70
55
55
40
35
25
4% input
GFP-IP
kDa
GFP
NLG2 CT WT
NLG2 CT PDZ-AAA
GFP
NLG2 CT WT
NLG2 CT PDZ-AAA
70
55
55
40
35
25
4% input
GFP-IP
kDa
GFP
NLG3 CT WT
NLG3 CT PDZ-AAA
GFP
NLG3 CT WT
NLG3 CT PDZ-AAA
70
55
55
40
35
25
SNX27
GFP–NLG CT
GFP
4% input
GFP-IP

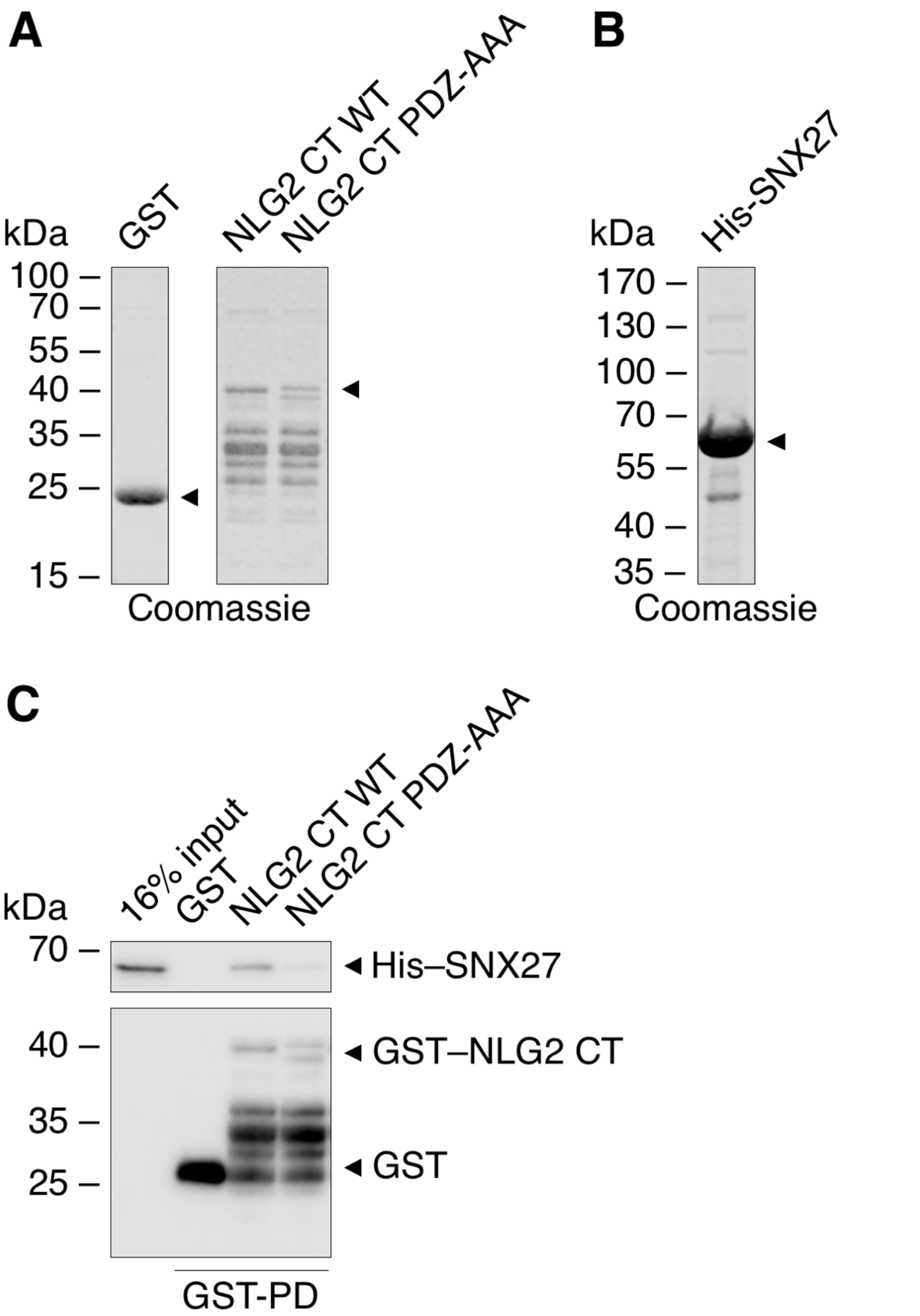
A
GST
NLG2 CT WT
NLG2 CT PDZ-AAA
kDa
100
70
55
40
35
25
15
Coomassie
B
His-SNX27
kDa
170
130
100
70
55
40
35
Coomassie
C
16% input
GST
NLG2 CT WT
NLG2 CT PDZ-AAA
kDa
70
His–SNX27
40
GST–NLG2 CT
35
25
GST
GST-PD

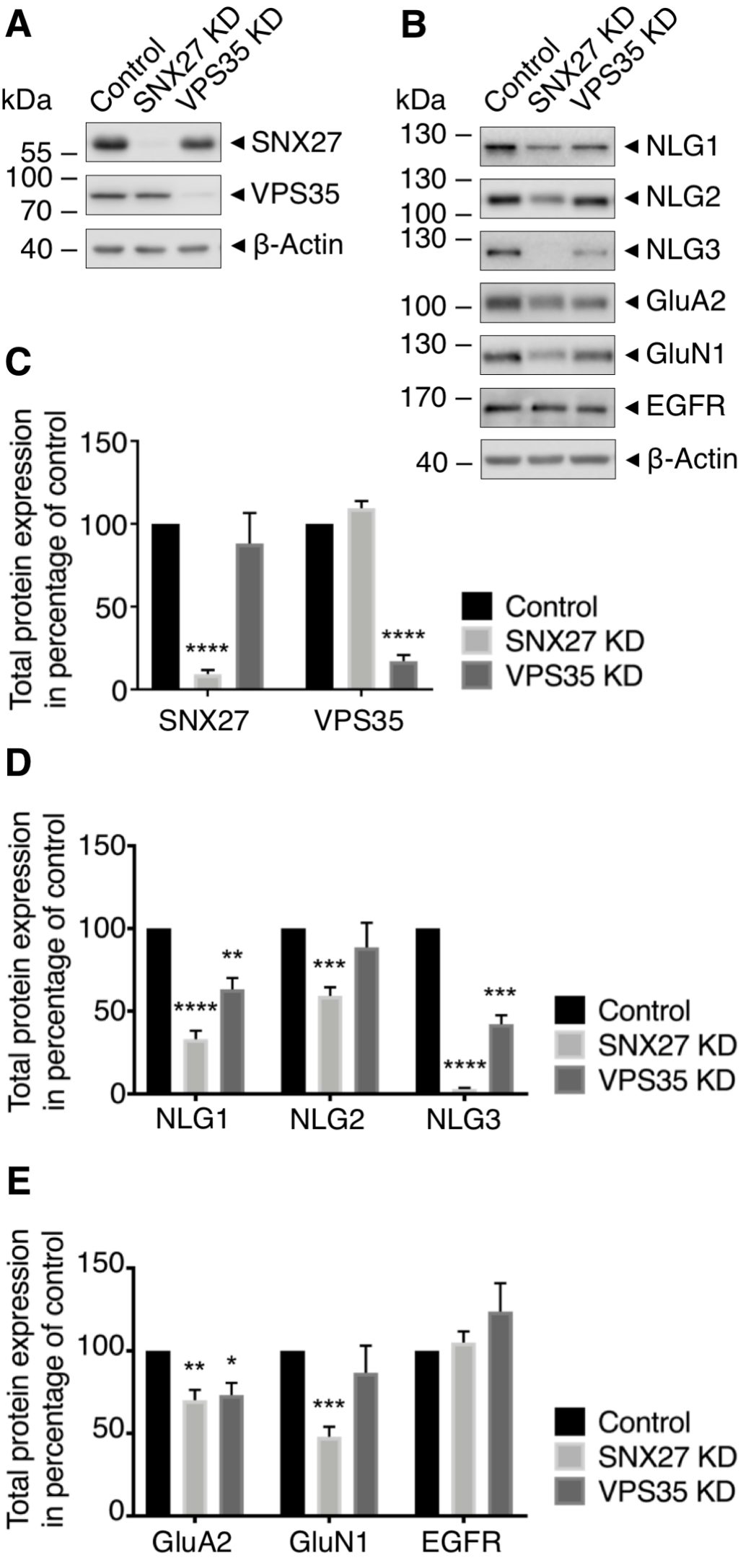
A
Control
SNX27 KD
VPS35 KD
kDa
55 –
100 –
70 –
40 –
SNX27
VPS35
β-Actin
B
Control
SNX27 KD
VPS35 KD
kDa
130 –
130 –
100 –
130 –
100 –
130 –
170 –
40 –
NLG1
NLG2
NLG3
GluA2
GluN1
EGFR
β-Actin
C
Total protein expression in percentage of control
150
100
50
0
****
****
SNX27
VPS35
Control
SNX27 KD
VPS35 KD
D
Total protein expression in percentage of control
150
100
50
0
****
**
***
****
***
NLG1
NLG2
NLG3
Control
SNX27 KD
VPS35 KD
E
Total protein expression in percentage of control
150
100
50
0
**
*
***
GluA2
GluN1
EGFR
Control
SNX27 KD
VPS35 KD

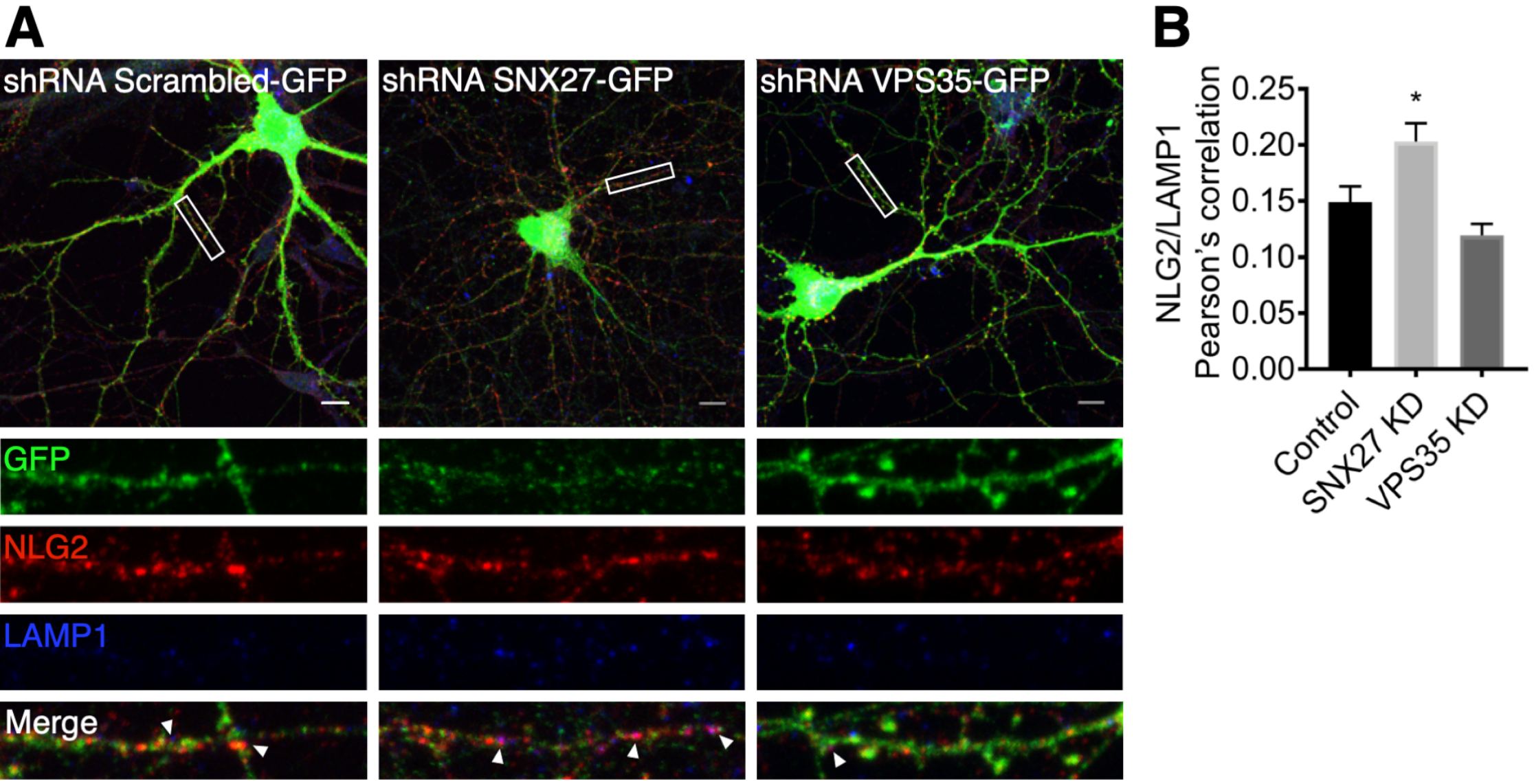
A
shRNA Scrambled-GFP
shRNA SNX27-GFP
shRNA VPS35-GFP
GFP
NLG2
LAMP1
Merge
B
NLG2/LAMP1
Pearson's correlation
0.25
0.20
0.15
0.10
0.05
0.00
*
Control
SNX27 KD
VPS35 KD

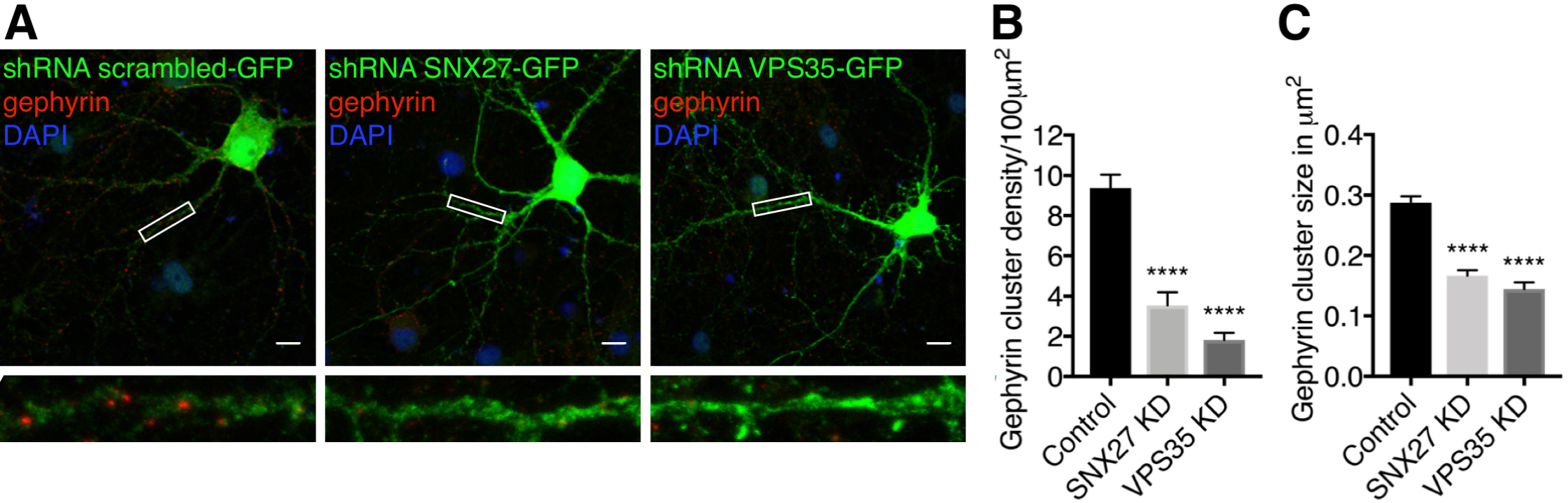
A
shRNA scrambled-GFP
gephyrin
DAPI
shRNA SNX27-GFP
gephyrin
DAPI
shRNA VPS35-GFP
gephyrin
DAPI
B
Gephyrin cluster density/100μm²
12
10
8
6
4
2
0
****
****
Control
SNX27 KD
VPS35 KD
C
Gephyrin cluster size in μm²
0.4
0.3
0.2
0.1
0.0
****
****
Control
SNX27 KD
VPS35 KD

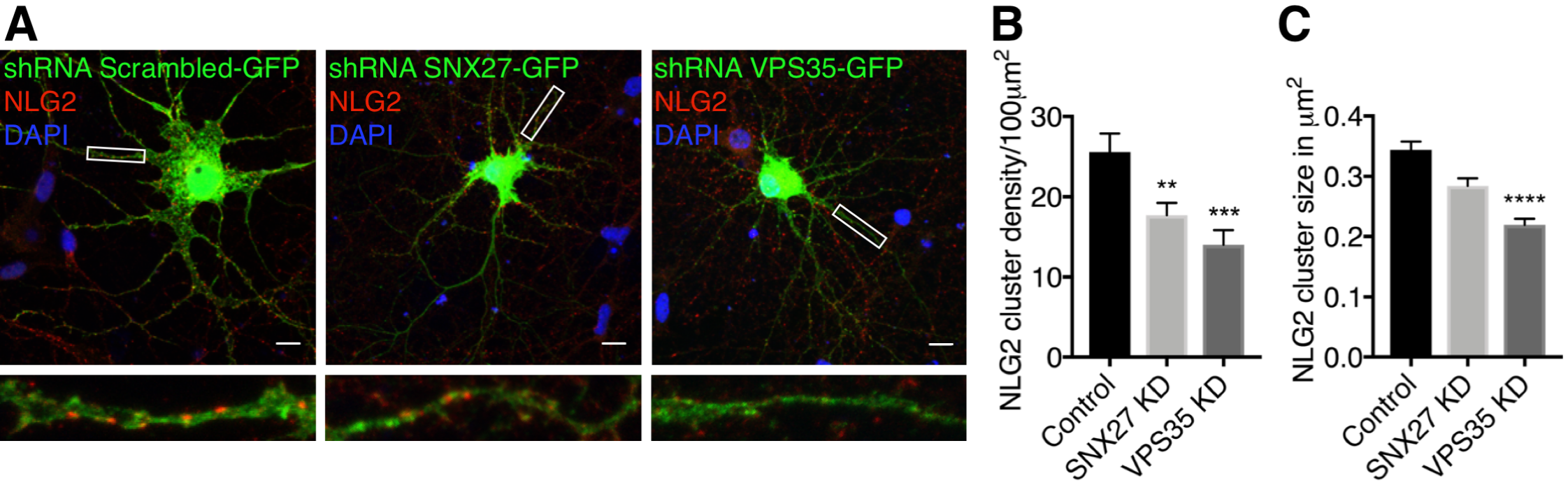
A
shRNA Scrambled-GFP
NLG2
DAPI
shRNA SNX27-GFP
NLG2
DAPI
shRNA VPS35-GFP
NLG2
DAPI
B
NLG2 cluster density/100μm²
30
20
10
0
**
***
Control
SNX27 KD
VPS35 KD
C
NLG2 cluster size in μm²
0.4
0.3
0.2
0.1
0.0
****
Control
SNX27 KD
VPS35 KD

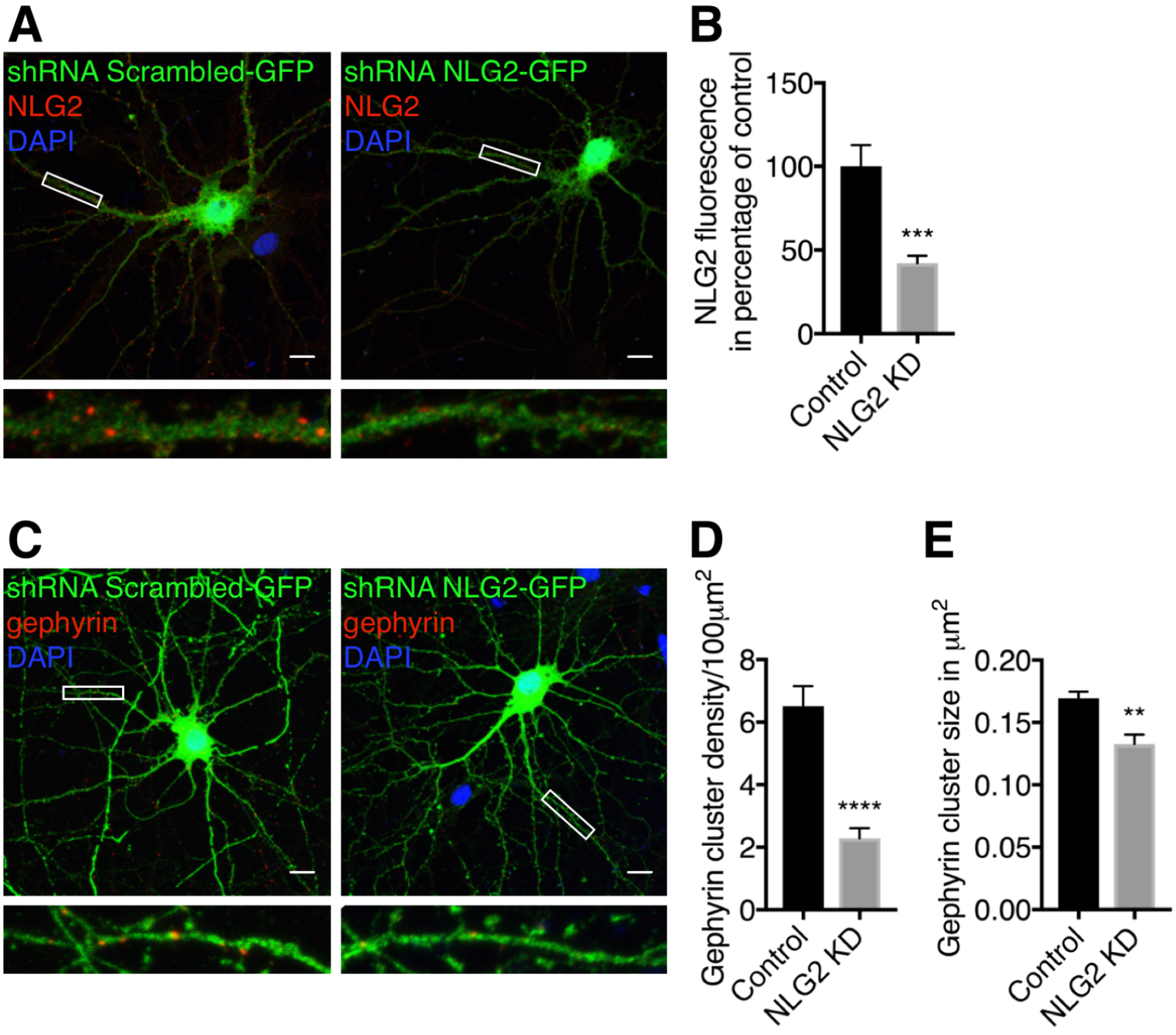
A
shRNA Scrambled-GFP
NLG2
DAPI
shRNA NLG2-GFP
NLG2
DAPI
B
NLG2 fluorescence in percentage of control
150
100
50
0
***
Control
NLG2 KD
C
shRNA Scrambled-GFP
gephyrin
DAPI
shRNA NLG2-GFP
gephyrin
DAPI
D
Gephyrin cluster density/100μm²
8
6
4
2
0
****
Control
NLG2 KD
E
Gephyrin cluster size in μm²
0.20
0.15
0.10
0.05
0.00
**
Control
NLG2 KD

A

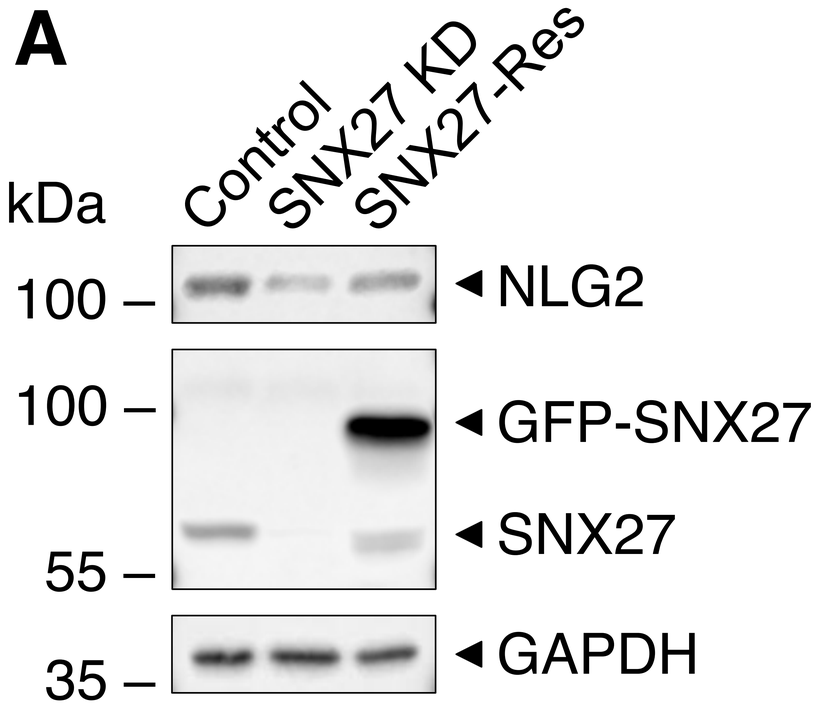
Control
SNX27 KD
SNX27-Res
kDa
100 –
NLG2
100 –
GFP-SNX27
SNX27
55 –
35 –
GAPDH

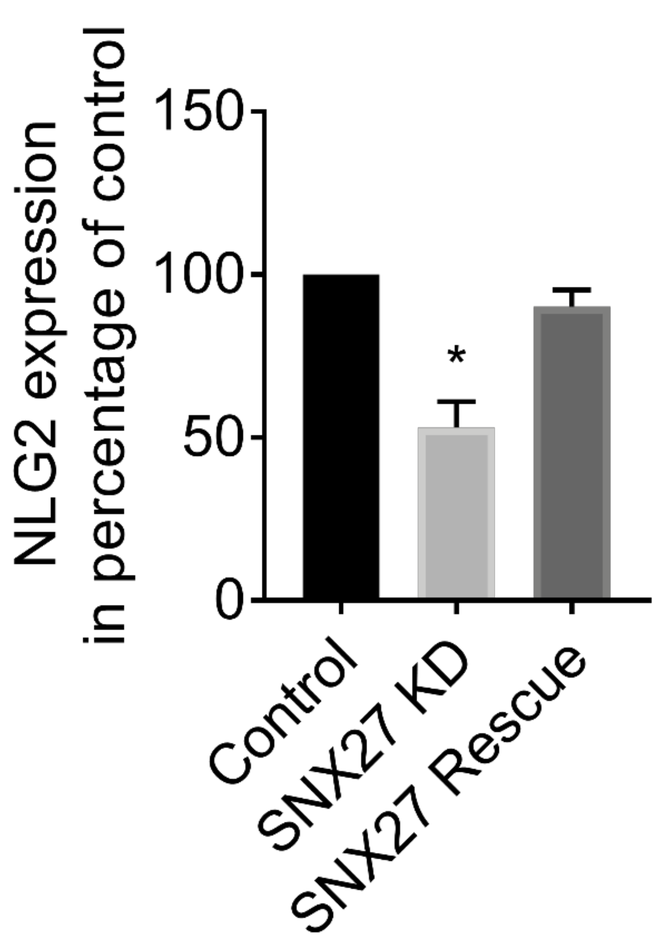
NLG2 expression
in percentage of control
150
100
50
0
*
Control
SNX27 KD
SNX27 Rescue

B

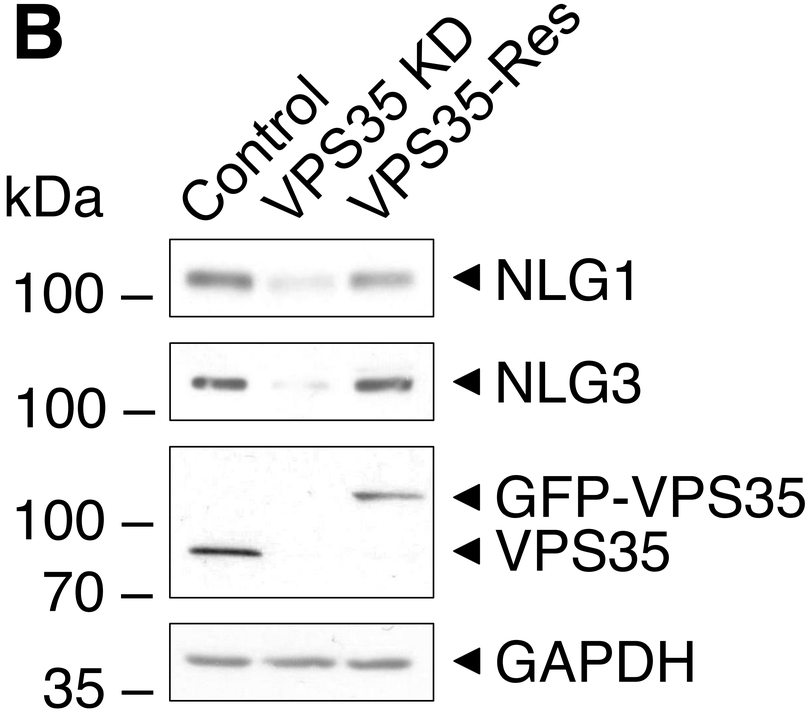
Control
VPS35 KD
VPS35-Res
kDa
100 –
NLG1
100 –
NLG3
100 –
GFP-VPS35
VPS35
70 –
35 –
GAPDH

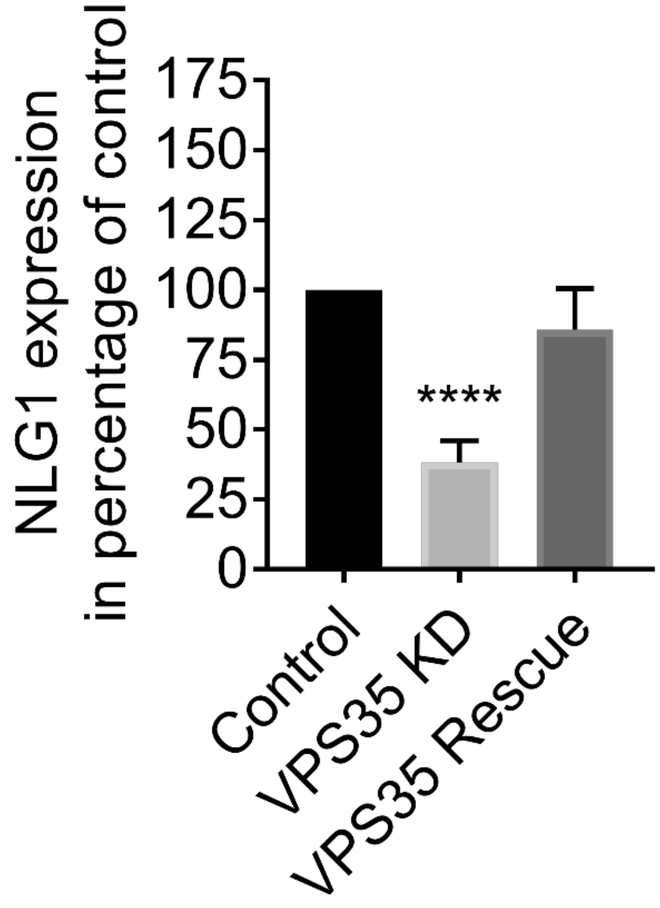
NLG1 expression
in percentage of control
175
150
125
100
75
50
25
0
****
Control
VPS35 KD
VPS35 Rescue

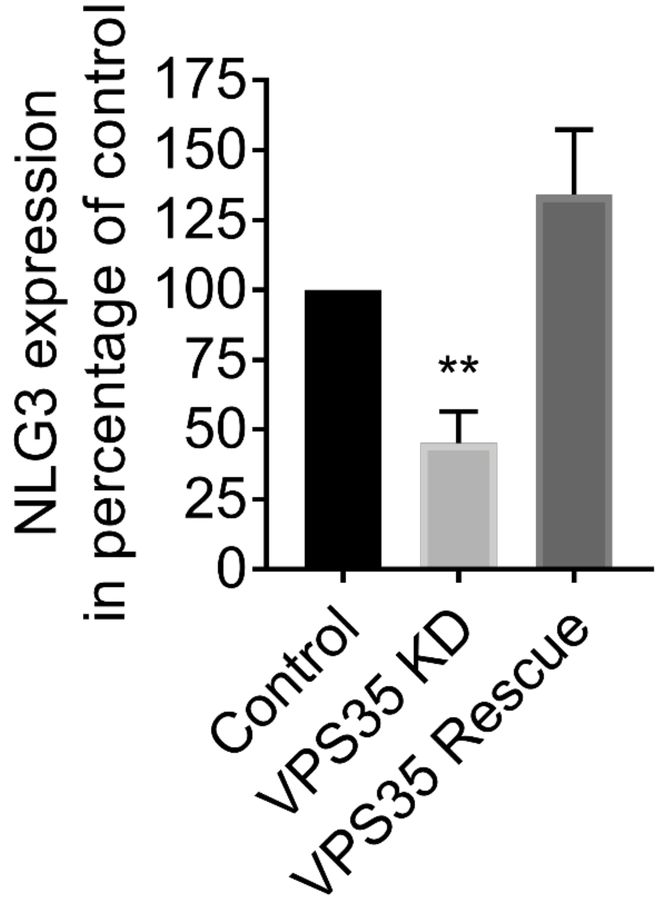
NLG3 expression
in percentage of control
175
150
125
100
75
50
25
0
**
Control
VPS35 KD
VPS35 Rescue

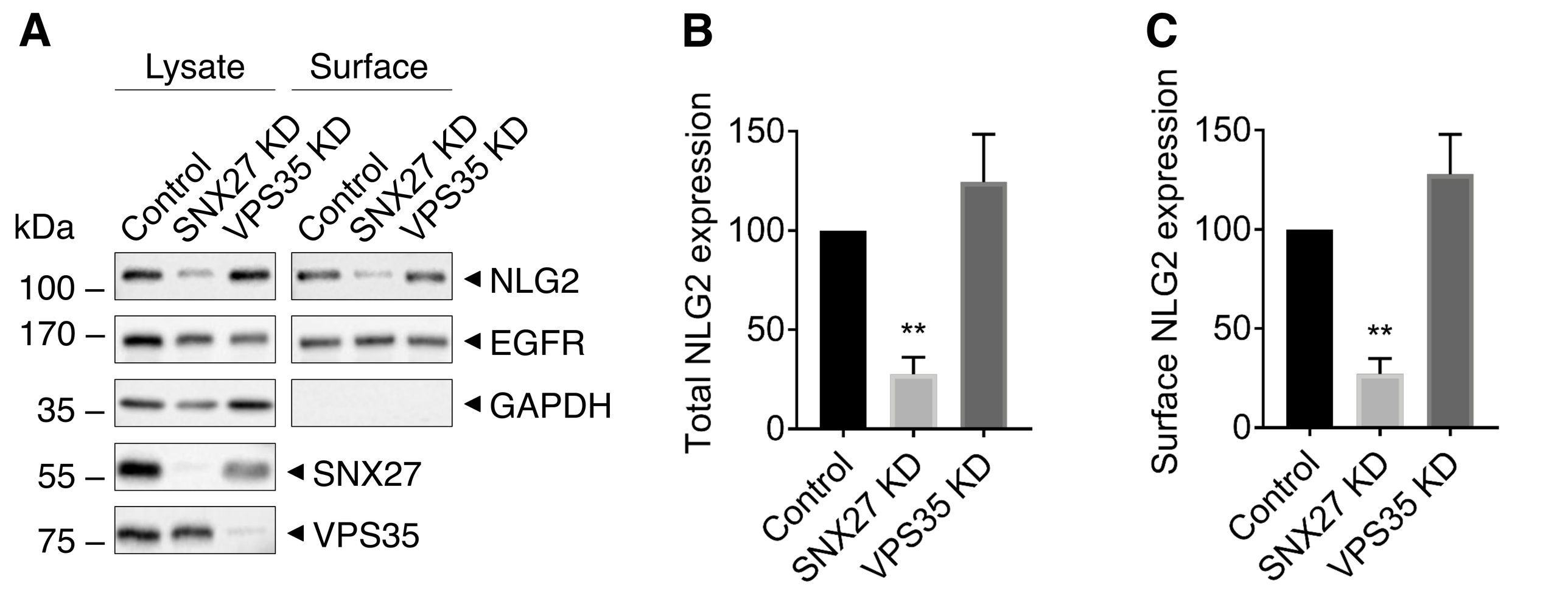
A
Lysate
Surface
Control
SNX27 KD
VPS35 KD
Control
SNX27 KD
VPS35 KD
kDa
100 –
170 –
35 –
55 –
75 –
NLG2
EGFR
GAPDH
SNX27
VPS35
B
Total NLG2 expression
150
100
50
0
**
Control
SNX27 KD
VPS35 KD
C
Surface NLG2 expression
150
100
50
0
**
Control
SNX27 KD
VPS35 KD

A

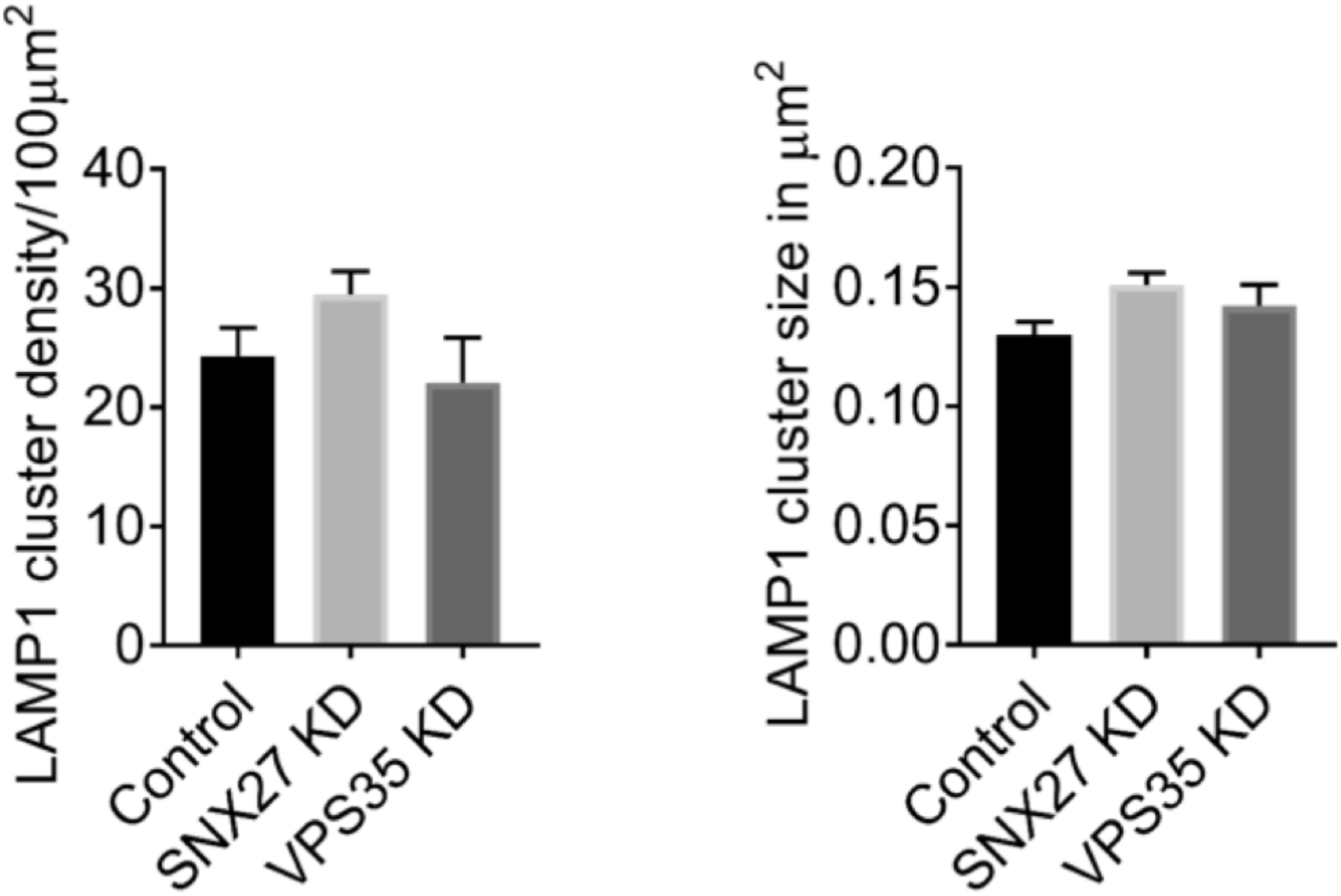
LAMP1 cluster density/100µm²
40
30
20
10
0
Control
SNX27 KD
VPS35 KD
LAMP1 cluster size in µm²
0.20
0.15
0.10
0.05
0.00
Control
SNX27 KD
VPS35 KD